**Atmospheric
Chemistry
and Physics
Discussions**

Mixing of Asian mineral dust with anthropogenic pollutants and its impact on regional atmospheric environmental and oceanic biogeochemical cycles over East Asia: a model case study of a super-duststorm in March 2010

J. Li[1], Z. Wang[1], G. Zhuang[2], G. Luo[1], Y. Sun[1], and Q. Wang[3]

[1]LAPC, Institute of Atmospheric Physics, Chinese Academy of Sciences, Beijing, China
[2]Center for Atmospheric Chemistry Study, Department of Environmental Science and Engineering, Fudan University, Shanghai, China
[3]Shanghai Environmental Monitoring Center, Shanghai, China

Correspondence to: Z. Wang (zifawang@mail.iap.ac.cn)

ACPD

12, 2743–2782, 2012

A model case study of a super-duststorm in March 2010

J. Li et al.

Title Page

Abstract	Introduction
Conclusions	References
Tables	Figures

|◄ | ►|
◄ | ►

Back | Close

Full Screen / Esc

Printer-friendly Version

Interactive Discussion

Abstract

Mixing of Asian mineral dust with anthropogenic pollutants allows pollutants (e.g. sulfate and nitrate) to be transported over longer distances (e.g. to the northern Pacific, even to North America) along with dust particles. This mixing therefore affects the atmospheric and oceanic environment at local, regional and even continental scales. In this study, we used a three-dimensional regional chemical transport model (NAQPMS) to examine the degree of mixing between Asian mineral dust and anthropogenic pollutants in a super-duststorm event during 19–22 March 2010. Influences of the mixing processes on regional atmospheric environmental and oceanic biogeochemical cycles were also investigated. A comparison with measurements showed that the model reproduced well the trajectory of long-range dust transport, the vertical dust profile, and the chemical evolution of dust particles. We found that along-path mixing processes during the long-range transport of Asian dust led to increasingly polluted particles. As a result, ∼60 % of the sulfate and 70–95 % of the nitrate in the downwind regions was derived from active mixing processes of minerals with pollutants sourced from the North China Plain and enhanced by transport over South China. This mixing had a significant impact on the regional-scale atmospheric composition and oceanic biogeochemical cycle. Surface HNO_3, SO_2 and O_3 were decreased by up to 90 %, 40 % and 30 %, respectively, due to the heterogeneous reactions on dust particles. Fe solubility rose from ∼0.5 % in the Gobi region to ∼3–5 % in the northwestern Pacific, resulting from oxidization of SO_2 on dust particles. Total Fe(II) deposition in the ocean region of East Asia reached 327 tons during the 4-day dust event, and created a calculated primary productivity of ∼520 $mgC\,m^{-2}\,d^{-1}$ in the Kuril Islands, which can support almost 100 % of the observed mean marine primary productivity in spring in this region (526 $mgC\,m^{-2}\,d^{-1}$).

Full Screen / Esc

Printer-friendly Version

Interactive Discussion

1   Introduction

Over the last few decades, China has experienced urbanization and industrialization processes on an unprecedented scale. More than 120 cities have populations of more than one million. This rapid growth in such a short period of time has not only led to a remarkable increase in material wealth and a higher standard of living, but has also caused serious so-called "complicated air pollution", which means various types of pollution (e.g. acid rain, coal smog, photochemical smog, duststorm and haze) are present together in China (He et al., 2002). The unique chemical transformation and transport processes in this "complicated air pollution" make emissions controls more difficult. In particular, the interaction between gas and aerosols creates major challenges for policy makers. Therefore, approaches to reduce "complicated air pollution" and its impact on other regions have already become the research focus for Chinese environmental scientists.

The mixing of Asian mineral dust with anthropogenic pollutants is one of the major research issues. This is because extremely high levels of sulfur dioxide (SO_2) and nitrogen dioxide (NO_2) in China allow dust particles to take up high levels of both these pollutants, leading to the formation of water-soluble sulfate and nitrate (Jordan et al., 2003). Compared with pure secondary anthropogenic sulfate and nitrate, sulfate and nitrate on dust can be transported over much longer distances (e.g. to the northern Pacific, even to North America), (Wilkening et al., 2000; Duce, 1980) along with dust particles. These pollutants alter the photochemistry, acid deposition and oceanic primary productivity along the pathway of long-range transport, through chemical transformation and dry/wet deposition (Tang et al., 2004; Zhuang et al., 2003; Jordan et al., 2003). Consequently, studying the mixing of Asian mineral dust with anthropogenic pollutants is crucial for a detailed understanding of the impact of China's anthropogenic emissions on the atmospheric and oceanic environments at local, regional and even continental scales.

The mineralogy of Asian dust particles consists primarily of carbonates ($CaCO_3$), quartz (SiO_2), feldspars, micas, clays and hematite (Fe_2O_3). Ca in Asian dust accounts for 39 % of seven crustal elements (Si, Al, Mg, Ca, Na and K), in contrast with Saharan dust particles where Ca only takes up 17 % (Krueger et al., 2004). The greater Ca concentration allows Asian dust particles to easily react with anthropogenic sulfuric and nitric acid, which consequently chemically alter the dust particles (Jordan et al., 2003). By collecting and analyzing aerosol samples over long time scales at North Pacific island stations, Zhuang et al. (1992) proposed a hypothesis for the coupling and feedback between natural iron (Fe) and anthropogenic S in the atmosphere and ocean. In this hypothesis, S(IV) in the form of SO_2 reacts with dust particles ($CaCO_3$) and is converted to SO_4^{2-}; meanwhile, absorption and chemical conversion of S(IV) acidifies particle surfaces and then mobilizes Fe(III) in dust particles (hematite) to dissolved Fe (Fe(II)), which is the limiting nutrient factor for primary productivity in certain oceanic regions. Zhuang et al. (1992) believed that this hypothesis can explain high Fe(II) and non-sea salt sulfate (nss-sulfate) observed in aerosol samples at a remote pacific station (Midway, Hawaii).

Partial evidence for Zhuang's hypothesis has been found in observations of Asian dust plume outflows in the Yellow Sea (China) and northwestern Pacific (a close down-wind region of China) since the late 1990s. Choi et al. (2001) reported that SO_4^{2-}, NO_3^-, Ca^{2+} and Mg^{2+} were the dominant water soluble ions in bulk dust aerosols in Seoul, and SO_4^{2-} and NO_3^- were primarily found in the coarse fraction associated with Ca^{2+} (Kim and Park, 2001). This is in contrast with non-dust observations suggesting that anthropogenic SO_4^{2-} and NO_3^- are associated with NH_4^+ in fine particles. Lidar observations showed that the aerosols were possibly an internal mixture of dust and sulfate during dusty days in the northeast Pacific (Sugimoto et al., 2002). Jordan et al. (2003) estimated that 43 % of sulfate came from Asian dust particles during an intensive aircraft-based aerosol sampling program as part of TRACE-P. Aerosol samples on the NASA DC-8 aircraft also revealed that the capture of SO_4^{2-} and NO_3^- by Asian mineral particles was accompanied by acid-mobilization of Fe (Meskhidze et al., 2003).

This acid-mobilization can increase Fe solubility from 0.5 % to 1–2 % within 3–5 days (Meskhidze et al., 2003). Excellent correlation between the marine primary productivity observed at two remote sites in the northwestern Pacific and dust storm frequency in China seems to support their conclusion (Deng et al., 2008).

5   Numerical modeling is a very useful tool for estimating the degree of mixing of minerals with anthropogenic pollutants (Tie et al., 2005). Various models have been used to estimate the contribution of China's anthropogenic emissions to this mixing process by comparing model results and observations in regions downwind of China's emissions (e.g. Korea, Japan and the northwestern Pacific). Lasserre et al. (2008) developed a

10   model for assessing this mixing. Using a regional model, Song and Carmichael (2001) estimated that chemical conversion of SO_2 on the surface of dust particles accounted for 10–40 % of SO_4^{2-} production in Asian dust plumes. Tang et al. (2004) found heterogeneous reactions on dust particles can produce >20 % of SO_4^{2-} and >70 % of NO_3^- under heavy dust loadings over the northwestern Pacific. Luo et al. (2005) and Fan

15   et al. (2006) also suggested that increasing SO_2 emissions alone could have caused significant Fe mobilization in the Northern Hemisphere oceans. However, the lack of model evaluation in China (the major region where minerals mix with pollutants) leads to large uncertainties in their estimations. A recent dust model intercomparison (DMIP) study over Asia found models differed greatly in their dust source regions, although

20   they agreed with each other in downwind regions, and suggested that modeling of dust transport and removal processes between China and Japan was one of the most important issues in improving dust modeling (Uno et al., 2006). In addition, greatly varied uptake coefficients are another origin of uncertainties (e.g. uptakes of nitric acid (HNO_3) varied greatly in the studies of Tang et al. (2004) and Tie et al. (2005), with val-

25   ues of 0.01 and 0.1, respectively). Therefore, a simulation evaluated by observations in China is urgently needed for assessing the extent to which mineral dust mixes with China's anthropogenic emissions.

Recent studies have extended observations into China. Sun et al. (2005) found SO_4^{2-}/Al and NO_3^-/Al ratios in dust particles in Beijing (Fig. 1) were 60 and 8 times

higher than those in surface soils of the Gobi Desert and Loess Plateau, respectively. They concluded that these high ratios in Beijing were attributed to the capture of SO_2 or HNO_3 by mineral dust during long-range transport (Sun et al., 2005). Meanwhile, Fe(II) in total Fe greatly increased, from 0.4 % to 1.3–5.3 %, during the long-range dust transport in Beijing (Zhang et al., 2005). By applying positive matrix factorization (PMF) combined with the enrichment factors method, Yuan et al. (2008) suggested that dust particles brought a lot of sulfate, but little nitrate, to Beijing. However, high concentrations of both sulfate and nitrate were observed in Xiamen, China (Fig. 1) during dusty days (Zhao et al., 2011). More evidence of the mixing of minerals with pollutants in China can be found in the literature (Zhuang et al., 2003; Wang et al., 2011a; Zhuang et al., 2010; Zhang et al., 2003). The above observations provide excellent opportunities for model simulations to estimate the extent to which dust mixes with China's anthropogenic emissions.

On 19–23 March 2010, a super-duststorm event occurred in China. In contrast to previous events, which have all occurred at mid-latitudes, this event covered the whole of eastern China from the Gobi desert (45° N) to South China Sea. Even at Xiamen city (24.5° N) in South China and on Dongsha Island (20° N) in the South China Sea, aerosol concentrations reached 990 µg m^{-3} and 300 µg m^{-3}, respectively, which are the highest levels in history (Zhao et al., 2011; Wang et al., 2011b). Remote sensing showed that this event lasted in eastern China for 4 days (Li et al., 2011b), which allowed dust particles to mix thoroughly with China's anthropogenic emissions.

The goal of this study is to estimate the extent to which Asian aerosols mixed with China's pollutants in the dust episode of 19–23 March 2010. We utilized a regional chemical transport model (NAQPMS) and evaluated its performance by comparison with in-situ and remote sensing observations in China. We also assessed changes of gas concentrations and inputs of Fe(II) to the ocean due to this mixing. In this paper, the description and validation of NAQPMS is presented in Sects. 2 and 3. Section 4 provides details of the mixing between dust particles and pollutants at the regional scale in East Asia. Section 4 also focuses on the chemical transformations on dust

Discussion Paper | Discussion Paper | Discussion Paper | Discussion Paper |

ACPD

12, 2743–2782, 2012

A model case study of a super-duststorm in March 2010

J. Li et al.

Title Page

Abstract | Introduction

Conclusions | References

Tables | Figures

◄ | ►►

◄ | ►

Back | Close

Full Screen / Esc

Printer-friendly Version

Interactive Discussion

particles during transport, and calculates the impacts of mixing on concentrations of atmospheric constituents and on marine primary productivity by dry/wet deposition of Fe(II) to the ocean.

2 Model description and setup

2.1 A brief description of the NAQPMS model

The Nested Air Quality Prediction Modeling System (NAQPMS) utilized in this study is a fully modularized three-dimensional regional Eulerian chemical transport model, driven by the meteorological model WRF-ARW 3.2. It reproduces the physical and chemical evolution of reactive pollutants by solving the mass balance equation in terrain-following coordinates (Li et al., 2008, 2007; Wang et al., 2006). It includes advection, diffusion and convection processes, gas/aqueous/aerosol chemistry, and parameterization of dry/wet deposition. An accurate mass conservative, peak-preserving algorithm is used to deal with advection (Walcek and Aleksic, 1998). The vertical eddy diffusivity is parameterized based on a scheme by Byun and Dennis (1995). The dry deposition module is the parameterization of Wesely (1989). The wet deposition and aqueous-phase chemistry section was based on the RADM mechanism used in the CMAQ version 4.6 (available at http://www.cmascenter.org/). Carbon-Bond Mechanism Z (CBM-Z), which is composed of 133 reactions for 53 species, has been embedded into NAQPMS to calculate the gas chemistry (Zaveri and Peters, 1999). NAQPMS employs an aerosol thermodynamic model (ISORROPIAI1.7) to calculate the composition and phase state of an ammonia-sulfate-nitrate-chloride-sodium-water inorganic aerosol (Nenes et al., 1998). A bulk yield scheme is used to deal with the formation of secondary organic aerosols (SOA) (Li et al., 2011a). Six SOAs, of which two are from anthropogenic precursors (toluene and higher aromatics) and four are from biogenic precursors (monoterpene and isoprene), are explicitly treated. Sea salt emissions ranging 0.43 to 10 µm are calculated following Athanasopoulou et al. (2008) with 4 size bins. Aerosol optical

Title Page

Abstract | Introduction

Conclusions | References

Tables | Figures

⏮ | ⏭

◀ | ▶

Back | Close

Full Screen / Esc

Printer-friendly Version

Interactive Discussion

depths are converted from mass concentrations using an external-mixture-based so-called "reconstructed extinction coefficient method" proposed by Malm et al. (2000) as part of the Integracy Monitoring of Projected Visual environment (IMPROVE) program.

2.2 Description of a unique dust deflation module

5　The generation of desert dust is critical in this study. Here, we applied a modified size-segregated dust deflation module designed by Wang et al. (2000) to simulate the long-range transport of Asian dust. The module was developed after detailed analysis of the meteorological conditions, landforms and climatology available in daily weather reports from about 300 local weather stations in northern China (Wang et al., 2000). It
10　has been successfully applied in the simulations of dust long-range transport, impact of dust on acid rain and dust-climate interactions (Wang et al., 2002; Yue et al., 2010). Recently, Luo et al. (2008) modified the soil dust emission intensity (F), considering soil categories, vegetation fraction percentages and snow/ice coverage, by introducing the following equation:

15　$$F = C_1 \times \frac{\rho_a}{g} \times E \times u^{*3} \left(1 + \frac{u_0^*}{u^*}\right) \times \left(1 - \frac{u_0^{*2}}{u^{*2}}\right) \times \left(1 - \frac{RH}{RH_0}\right) \qquad (1)$$

where F is the dust flux (kg m^{-2} s^{-1}). The constant C_1 is set to 1.0×10^{-5}. ρ_a (kg m^{-3}) and g (m^2 s^{-2}) are the air density and acceleration due to gravity. E is the weighting factor of dust loading for different soil categories, vegetation fractions and snow/ice coverage. In this study, soil categories, vegetation fractions and snow/ice coverage
20　are derived from Moderate Resolution Imaging Spectrometer (MODIS) data. Figure 1 shows the distribution of calculated E in this study. u^* and u_0^* are the fraction and threshold friction velocities. Here, u_0^* is set to 0.45, 0.35 and 0.6 m s^{-1} in the Gobi, China Loess and Hunshandak deserts, respectively. These values were obtained from observations by Zhu and Zhang (2010). u_0^* in other dust source regions is set as
25　0.4 m s^{-1} as suggested by Yue et al. (2010). RH and RH$_0$ represent relative humidity

and its threshold value. In this study, RH_0 is set to 40 %. The dust particle size is divided into 4 size bins covering the range 0.43–10 µm in diameter.

2.3 Heterogeneous chemistry

In this study, 28 heterogeneous reactions are considered when simulating the mixing of aerosols with pollutant gases. Table 1 lists the all reactive uptake coefficients, some of which consider the effects of relative humidity (e.g. reactions with nitric acid on dust particles). The first-order rate constant (k_{het}) is calculated by uptake coefficients (γ) and surface area density of particles (A) using the following equation suggested by Jacob (2000):

$$k_{het} = \left(\frac{r}{D_g} + \frac{4}{cr} \right)^{-1} \times A \tag{2}$$

where r is the black carbon and sulfate mean radius, D_g is the gas phase diffusion coefficient, $c = \left(\frac{8kT}{m} \right)^{0.5}$ is the mean molecular speed of the gas, γ is the uptake coefficient and A is the surface area density of the particles.

The heterogeneous reactions of SO_2 and HNO_3 (HR12 and HR19 in Table 1) acidulate dust particles and subsequently mobilize Fe(III) in the dust particles (hematite) to dissolved Fe. Therefore, the fraction of dissolved Fe in total Fe is regarded as an important indicator of the mixing of mineral dust with pollution. In this study, the solubility of Fe in dust aerosols is parameterized by a two-step mechanism proposed by Fan et al. (2006). In this mechanism, dust/iron is divided into three types: fresh, coated and dissolved (for Fe). In the first step, gas uptakes convert dust particles from fresh to coated by the heterogeneous reactions HR12 and HR19. The rate coefficient is calculated from $k_s[SO_2] + k_n[HNO_3]$, where k_s and k_n represent the first order rates of HR19 and HR12. In the second step, Fe(III) in the coated dust is transferred to dissolved Fe (Fe(II)). The production rate of Fe(II) is calculated from $R_{Fe} = R_d A n M / w$, where R_{Fe} is grams of Fe dissolved per gram of Fe(III) per second, R_d is the dissolution rate per unit

surface area, A is the specific surface area of hematite ($m^2\,g^{-1}$), $n = 2$ (moles Fe/moles hematite), M is the gram-molecular weight of Fe, and w is the mass fraction of Fe in hematite (i.e. 0.7). Here, R_d and A are set as $1 \times 10^{-10}\,mol\,m^{-2}\,s^{-1}$ and $100\,m^2\,g^{-1}$ as suggested by Fan et al. (2006) and Duckworth and Martin (2001). Obviously, the conversion of dust from fresh to acid-coated depends on local SO_2 concentrations, while the formation of dissolved Fe does not. Besides the heterogeneous chemistry, the effects of radiation process and cloud process on Fe-mobilization are also considered based on the scheme devised by Luo et al. (2005). Here the Fe solubility is assumed to have a lower limit of 0.5 % (Fan et al., 2006).

In this study, SO_4^{2-} and NO_3^- taken up by natural particles due to heterogeneous reactions are internally mixed with natural particles (dust and sea salt), while anthropogenic SO_4^{2-} and NO_3^- are externally mixed.

2.4 Model setup

Figure 1 shows the NAQPMS model domain used in this study, which is composed of two nested domains. The coarser domain is $7760 \times 6160\,km$ on a Lambert conformal map projection with 80-km grid resolution. The nested domain is divided into 148×160 horizontal grids with 20 km resolution. Vertically, the model uses 20 terrain-following layers from the surface to 20 km a.s.l.

The first meteorological guess fields and boundary conditions for the coarse domain for every 6 h are obtained from NCAR/NCEP FNL reanalysis data ($1° \times 1°$). Nudging, or four dimensional data assimilation (FDDA) (OTTE, 2008), consisting of 6-h 3-D analyses of temperature, water vapor mixing ratio and horizontal wind components for both domains, and 6-h surface analyses of horizontal wind components for the coarse domain, were used with nudging coefficients of 3.0×10^{-4} for the wind, temperatures and humidity fields of the coarse and nested domains. In this study, The Yonsei University (YSU) Boundary Layer (BL) scheme is used for calculating BL height. The surface layer and land surface schemes are the MM5 similarity and Noah Land Surface schemes, respectively.

The anthropogenic emissions of air pollutants (fossil fuels, biofuels and industrial emissions) in Asia are derived from the year 2006 bottom-up Regional Emission inventory in Asia (REAS) data at (0.5° × 0.5°) resolution (Ohara et al., 2007). The initial and boundary conditions are taken from a global chemical transport model MOZART-V2.4 with 2.8° resolution. The mass fraction of Fe(III) in dust particles is set as 2.8 % in this study, following Zheng et al. (1994).

The simulation started at 00:00 UTC on 10 March 2010 and ran through to the 24 March 2010. The first 5 days are regarded as the spin-up period, used to reduce the influence of initial conditions.

3 Model validation

Before validating concentrations of simulated dust particles and pollutants, we compare the predicted and observed hourly averaged meteorological variables (temperature, relative humidity and wind) during 19–23 March 2010 (figure not shown). The results show the model successfully reproduced the synoptic features of the meteorological variables, notably the change of wind direction from northward to southward during the dust episode.

3.1 Comparison with satellite retrievals

Figure 2 presents the aerosol optical depth (AOD550) at 550 nm retrieved by MODIS (available at http://gdata1.sci.gsfc.nasa.gov/daac-bin/G3/gui.cgi?instance_id=MODIS_ DAILY_L3) and the AOD550 simulated by NAQPMS during the 19–23 March 2010. In general, the simulation reproduced the long-range transport of dust particles and anthropogenic aerosols over East Asia reasonably well over the study period. On 19 March, a duststorm episode started over the Gobi desert, as shown in Fig. 2e. This was associated with the formation of a strong Siberian-Mongolian high pressure system and a much stronger westerly wind in the Gobi, which entrained desert sand into

the atmosphere (figure not shown). Unfortunately, MODIS data are missing over the Gobi due to either the lack of interorbital coverage or cloud contamination (Fig. 2a). However, the aerosol index measured by OMI (Ozone Monitoring Instrument) captured this outbreak of dust deflation over the Gobi (Li et al., 2011b). On 20 March, both the model and MODIS revealed that dust particles moved southeasterly to the North China Plain, the Gulf of Bohai and the Korean peninsula (Fig. 5b, f), where AOD550 was generally greater than 2. On 21 March, the dust plume and cold front advanced further, reaching southern China (including Xia'men City) and Taiwan. Over the ocean, a narrow plume extended from Taiwan to the southwest of Japan. Due to relatively calm winds associated with the southeastward-moving high, dust particles still accumulated in central China and the Yangtze River delta (Fig. 5c, g). On 23 March, MODIS showed a relatively high AOD500 belt in the mid-latitudes, which we attribute to the combination of weakened dust and anthropogenic particle (e.g. BC, sulfate and nitrate) concentrations. This pattern is well reproduced by the simulation, which indicates good model performance with respect to both dust and anthropogenic particles.

3.2 Comparison with ground-based observations

Simulated concentrations of PM_{10} (particles on the order of $\sim 10 \, \mu m$ or less) at six stations covering most of east China (20° N~40° N) are compared with observations in Fig. 3. The observed daily averages at five sites on mainland China are converted from the Air Pollution Index (API) using the method of Li et al. (2011b). At Taipei, daily PM_{10} is directly calculated using the 24-hourly averaged values. Note that API has an upper limit of 500, which means this value of 600 $\mu g \, m^{-3}$ is a "saturation" maximum value. As shown in Fig. 3, the model yielded good agreement with observations. Concentrations of PM_{10} abruptly increased on 20, 21 and 22–23 March in north China (Beijing and Jinan), the Yangtze River Delta (Shanghai and Nanchang) and south China (Xiamen and Taipei), respectively. The model correctly captured this pattern and showed a similar peak magnitude (e.g. in Taipei, Shanghai, and Nanchang). In Beijing and Jinan, the model slightly overestimated the peak. This is attributed to the imposed upper

limit of API (600 µg m^{-3}). However, other observations revealed a peak of 3000 µg m^{-3} hourly concentrations (personal communication), which are consistent with this simulation (3300 µg m^{-3}). The simulation under predicted observed PM$_{10}$ in Xiamen city, probably due to the stronger simulated deposition processes.

Lidar observations provide a good opportunity to evaluate the model's ability to predict vertical aerosol profiles. Figure 4 shows the observed and simulated vertical profiles of dust extinction coefficients during 15–24 March 2010. The two-wavelength Mie-scattering lidar observations (1064 nm and 532 nm) are taken from the National Institute for Environmental Studies (NIES), Japan (http://www-lidar.nies.go.jp/). Clearly, the simulation agrees well with the overall evolution of the Lidar extinctions pattern. During the 19–22 March dust episode, the dust plume at three stations was constrained below 3 km and maintained a rather homogeneous profile. At Nagasaki and Hedo, another dust event on 19 March in the 1–3 km layer was accompanied by observations of a few dust particles on the ground. The model also captured this phenomenon.

Figure 5 compares observed and simulated SO$_2$ and NO$_2$ in Beijing and Shanghai during 15–24 March 2010. The model agrees with observations quite well, except for a significant underestimation of NO$_2$ in Shanghai. The correlation coefficients are in the range 0.49–0.67. In particular, the decrease of SO$_2$ and NO$_2$ concentrations in the dust episode is captured by the model. The underestimation of NO$_2$ in Shanghai is caused by the uncertainties of the REAS emission inventory (0.5° × 0.5°) in the Yangtze River Delta.

The model's ability to simulate sulfate and nitrate in non-dust and dust periods is critical in assessing the mixing extent in this study. Figure 6 presents a comparison of simulated and observed sulfate and nitrate in Shanghai and Xiamen during the pre-dust, dust and after-dust periods. Both the model and observations show that SO$_4^{2-}$ and NO$_3^-$ significantly increased by factors of 2–3 times those in the pre-dust and after-dust periods at both sites. The simulation clearly indicates that the mixing of minerals with anthropogenic pollutants during the long-range transport played the dominant role in this increase, while anthropogenic SO$_4^{2-}$ and NO$_3^-$ particles decreased along with

their precursors (SO_2 and NO_2) during the duststorm (Fig. 5). In the next section, we will discuss where the mixing of minerals with pollutants occurred (Figs. 7 and 8). Figure 6 also shows that the simulation underestimated the concentration of sulfate at Xiamen. This was caused by the underestimation of dust particle concentrations (as shown in Fig. 3). In fact, the simulated mass fraction of sulfate (5.2 %) in the total particles is consistent with observations (4.8 %).

Unfortunately, few observations of the size distribution of dust particles are available for this dust episode, although we were able to collect fine and coarse particles from Shanghai and Xiamen (Table 2). These results showed the deposited particles coarsened as the plume moved south. The mass fraction of fine particles in Xiamen was twice of that in Shanghai. The model reproduced this pattern reasonably well. The simulated fine particle fraction (47.9 %) in Xiamen was very close to the observation (43 %). However, the model overestimated the mass fraction of fine particles in Shanghai. This is likely caused by the local re-suspension of deposited dust particles. Shanghai is closer to the dust source regions than Xiamen, and hence depositions contained more coarse particles. The strong wind in the dust episode may have re-entrained more coarse deposited particles into the atmosphere in Shanghai. Yuan et al. (2008) found that this re-suspension contributed 10–30 % of total TSP [total Total suspended particles] in Beijing. Most dust models, including NAQPMS in this study, fail to reproduce the re-suspension process.

In general, the above model validation indicates that NAQPMS is capable of reproducing the temporal and spatial distributions of observed dust particles and anthropogenic pollutants. It can also reproduce the chemical evolution of pollutants on dust particles. The reasonable performance provides some confidence in the model-derived results.

4 Results and discussion

4.1 Level of mixing between mineral dust and pollutants

As shown in Fig. 6, SO_4^{2-} resulting from the mixing of minerals with pollutants contributed more than 50 % to the total sulfate in both Shanghai and Xiamen. Figure 7 shows the chemical evolution of SO_4^{2-}, NO_3^- and dissolved Fe along the back-trajectories during dusty days. The back trajectories are calculated by a Hybrid Single-Particle Lagrangian Integrated Trajectory (HYSPLIT v4) model based on WRF output with 80 km resolution (http://ready.arl.noaa.gov/HYSPLIT.php). For Shanghai, Fig. 7a–c shows dust particles stayed fresh and experienced no significant mixing with pollutants until they arrived on the North China Plain (30–40° N, 110–120° E). The concentration of SO_4^{2-} taken up by dust particles significantly increased from $5\,\mu g\,m^{-3}$ to $20\,\mu g\,m^{-3}$ when the air mass reached the North China Plain. Both NO_3^- on dust particles and Fe solubility show a similar pattern to SO_4^{2-}. This indicates that high concentrations of anthropogenic pollutants on the North China Plain extensively coated these fresh dust particles transported from the Gobi desert, due to heterogeneous reactions (Table 1). The fraction of Fe(II) in total Fe in Shanghai was in the range 0.8–1.5 %, which was less than previously observed values in a duststorm event in Beijing in April 2002 (1.3–5.3 %) (Zhang et al., 2005). This is likely to be due to the underestimation of the dissolution rate of Fe on dust particles (R_d) in this study. The different transport pathway between two episodes is another likely cause. In our study, after the air mass passed Shanghai, mixed dust particles were transported to South China (e.g. Xiamen) along the coast line, where high relative humidity promoted the heterogeneous reactions. Consequently, anthropogenic gases (SO_2 and HNO_3) were more rapidly converted to SO_4^{2-} and NO_3^- on the dust particles. The fraction of Fe(II) reached 1.6–5.3 % in Xiamen, which indicates that mixing in South China was more active than in North China.

Title Page

Abstract | Introduction

Conclusions | References

Tables | Figures

◄ | ►

◄ | ►

Back | Close

Full Screen / Esc

Printer-friendly Version

Interactive Discussion

Similarly to the fraction of Fe(II) in total Fe, the fractions of SO_4^{2-} and NO_3^- captured by dust particles in total sulfate and nitrate are regarded as indices of the degree of mixing. Figure 8 shows the spatial distributions of the percentages (at the surface) of SO_4^{2-} and NO_3^- captured by dust particles in total sulfate and nitrate masses during the dusty period. Fe(II) in total Fe is also shown. Here the dusty days are defined as the periods with total dust levels greater than $100\,\mu g\,m^{-3}$, as suggested by Tang et al. (2004). It was found that SO_4^{2-} mixing with minerals contributed over 60 % to total sulfate over eastern China and its downwind regions (northwestern Pacific), while its contribution was only 10–20 % in the Gobi. The contribution of mixed NO_3^- was 70–95 % over the Gobi, eastern China and northwestern Pacific, which indicates that the level of mixing of NO_3^- was higher than that of SO_4^{2-}. This is partially due to the higher HNO_3 uptake (HR12 in Table 1) on dust particles than that of SO_2 (HR19 in Table 1), particularly in South China and the northwestern Pacific with high RH conditions (Jordan et al., 2003). The more complicated origin of SO_4^{2-} is likely to be another cause. In the semi-arid area of the Chinese Loess Plateau, sulfate usually covers 0.01–0.45 % of soils or sands. In plumes with high dust loadings (i.e. dust source regions), the emitted mineral dust significantly contributes to total sulfate mass, which decreases the fraction of mixed sulfate. Our results for SO_4^{2-} are higher than those in previous studies. For example, Tang et al. (2004) estimated that dust enhanced sulfate by up to 25 % during a duststorm event in 2001. This indicates the strong mixing intensity of the duststorm event during 19–22 March 2010.

The fraction of Fe(II) in total Fe shows a gradual increase from the Gobi (<0.5 %) to northwestern Pacific (~3–5 %) (Fig. 8c). This reflects the oxidation of SO_2 on dust particles during the long-range transport and is consistent with many previous observations. Zhuang et al. (1992) found Fe(II) only accounted for 0.4 ± 0.3 % of total Fe in the Chinese Loess. When dust particles were transported from the Gobi to Beijing, a megacity at the edge of the North China Plain (a highly polluted region), the fraction reached 1.3–2.6 % (Zhuang et al., 2003). Over the remote mid-Pacific, Fe(II) on Asian dust particles continued rising, to 5–10 %. The simulation captures this observed

increase of Fe solubility with distance from dust source regions (i.e. the Gobi) well.

4.2 Regional dust influences

In order to investigate the influences of dust on the regional atmospheric and oceanic environment, a sensitivity simulation without mixing processes was performed. The
5 difference between the sensitivity and base simulation reveals the influence of dust.

4.2.1 Influences on concentrations of atmospheric tracer gases

As well as aerosol compositions, the mixing of minerals with anthropogenic pollutants also alters the regional-scale concentrations of gaseous pollutants. Figure 9 shows the averaged influence of dust on surface HNO_3, O_3 and SO_2 during 19–22 March
10 2010. The average HNO_3 decrease due to heterogeneous reactions was 20–90 %, with the strongest decrease occurring in western China and in the Pacific to the south and east of Japan (up to 80 %–90 %) (Fig. 9a). The distribution of the SO_2 decrease was similar to that of HNO_3, but its impact was smaller (5–40 %) (Fig. 9c). Moreover, the impact area was much smaller. For O_3, the decrease was in the range 5–30 %
15 (Fig. 9b). An interesting point is that the influences of dust in polluted regions (e.g. the North China Plain: 30–40° N and l10–120° E) were much smaller than those in remote regions. This is because high emission rates and complex photochemical systems on the North China Plain can offset part of their heterogeneous losses. Our estimations are consistent with the study of Tang et al. (2004), who estimated that surface HNO_3,
20 SO_2 and O_3 decreased by 95 %, 20 % and 20 %, respectively, due to heterogeneous reactions on dust particles.

4.2.2 Influences on marine primary productivity

A large number of studies have demonstrated that dissolved iron (Fe(II)) in surface seawater is the limiting nutrient factor for primary productivity in high-nitrate low-chlorophyll
25 (HNLC) regions of ocean. Deposition of Asian mineral dust is thought to be the major

Title Page

Abstract | Introduction

Conclusions | References

Tables | Figures

◄ | ►►

◄ | ►

Back | Close

Full Screen / Esc

Printer-friendly Version

Interactive Discussion

source of Fe(II) in the Pacific. The Fe(II) deposited into the ocean may substantially affect ocean productivity, and by altering the uptake of carbon dioxide through the ocean, may even affect the global greenhouse effect (Zhuang et al., 2003). Figure 10 shows simulated dry, wet and total deposition of Fe(II) during this duststorm event. In order to isolate the impact of mixing processes on Fe(II) deposition, Fe(II) deposition calculated in a sensitivity simulation without mixing processes is summarized in Table 3.

Fe(II) deposition in the ocean off East Asia ranged from 20 to 100 μg m^{-2} (Fig. 10a). The largest depositions occurred in the East China Sea (40–60 μg m^{-2}, and in the Sea of Japan and the Kuril Islands (100 μg m^{-2}, which comprised dry deposition (Fig. 10b) and wet deposition (Fig. 10c), respectively. As shown in Fig. 10b and c, dry deposition dominated the total deposition of Fe(II) close to the Chinese mainland, while wet deposition played a more important role in the far downwind ocean. Table 3 lists atmospheric deposition fluxes of Fe(II) to the ocean in base and sensitivity simulations. Clearly, the mixing of minerals with anthropogenic pollutants significantly increased the deposition of Fe(II).

Assuming that all the Fe(II) transported and deposited into oceans are bioavailable to phytoplankton. The input can be converted to carbon uptake by using a cellular Fe:C ratio of 10 μmol mol^{-1} in the subarctic Pacific (e.g. the Kuril Islands: 150° E, 45° N) where observed concentration of dissolved Fe (e.g. the Kuril Islands: 150° E, 45° N) was about 0.2 nmol l^{-1} (Sunda and Huntsman, 1997). If we neglect removal by abiotic scavenging, our simulated 100 μg m^{-2} Fe(II) deposition (over 4 days) in the Kuril Islands can create a marine primary productivity of $\sim$520 mgC m^{-2} d^{-1}, which can support almost 100 % of the observed mean marine primary productivity in spring in this region (526 mgC m^{-2} d^{-1}) (Imai et al., 2002). This indicates that dissolved Fe deposition mostly affected the marine primary productivity during this duststorm event. Our results also support previous studies which claimed subarctic Pacific is one of the major HNLC regions in the world and inadequate dissolved iron (Fe(II)) input was the limiting nutrient factor (Martin et al., 1988; Zhuang et al., 2003).

Title Page

Abstract | Introduction

Conclusions | References

Tables | Figures

|◄ | ►|

◄ | ►

Back | Close

Full Screen / Esc

Printer-friendly Version

Interactive Discussion

5   Conclusions

The objective of this study was to examine the extent to which Asian mineral dust is mixed with anthropogenic pollutants in a super duststorm event during 19–22 March 2010. Meanwhile, influences of mixing processes on regional atmospheric environ-
5 mental and oceanic biogeochemical cycles were also investigated.

A variety of observational data including in-situ ground-based concentrations of PM_{10} and its chemical compositions, extinction coefficient data of dust particles from two-wavelength Mie-scattering lidar observations, and MODIS satellite AOD550 retrievals were used to validate the performance of the NAQPMS model. The model validation
10 indicates that NAQPMS is capable of reproducing the long-range transport of dust particles from the Gobi desert to the South China Sea and northwestern Pacific. The vertical profile of dust plumes is also reproduced well. Even more importantly, NAQPMS captures the chemical evolution of dust particles during the long-range transport: for example, the increasing concentrations of sulfate, nitrate and Fe(II).
15 We found that mixing processes along the trajectory of the long-range transport of Asian dust strongly increased pollutant levels in the dust particles. In Shanghai, a megacity located in the Yangtze River Delta, SO_4^{2-} and NO_3^- levels captured by minerals reached ~15 and $10 \, \mu g \, m^{-3}$, respectively. Even in southern China (Xiamen City), the mixing processes contributed ~60 % of the SO_4^{2-} and ~90 % of the NO_3^-, with the help
20 of high RH. Analysis based on back trajectories indicates that the active mixing stared in the North China Plain, which is consistent with the distribution of anthropogenic emissions. In general, mixing SO_4^{2-} with minerals made an overall contribution to total sulfate of ~60 % over eastern China and its downwind regions (northwestern Pacific), while its contribution was only 10–20 % in the Gobi. The equivalent contribution of
25 mixed NO_3^- was 70–95 % over the Gobi, eastern China and northwestern Pacific. The Fe solubility (the fraction of Fe(II) in total Fe) resulting from oxidization of SO_2 on dust particles showed an increase with distance from dust source regions, of the order of ~0.5–5 %.

The mixing of minerals with pollutants could have important impacts on the atmospheric composition and marine primary productivity over East Asia. In this study, dust particles significantly decreased surface HNO_3, SO_2 and O_3 by up to 90 %, 40 % and 30 %, respectively, due to the heterogeneous chemistry. We estimated that the Fe(II) deposition in the ocean off East Asia totally reached 327 tons during the 4-day dust event, mostly due to the mixing of minerals with pollutants. The largest deposition occurred in the East China Sea (40–60 μg m^{-2}), and in the Sea of Japan and Kuril Islands (100 μg m^{-2}. A rough estimation showed that our simulated 100 μg m^{-2} Fe deposition (over 4 days) in the subarctic Pacific(e.g. Kuril Islands) can create a marine primary productivity of $\sim$520 mgC m^{-2} d^{-1}, which is consistent with the observed mean marine primary productivity in spring in this region (526 mgC m^{-2} d^{-1}. Our results suggest that the Fe(II) deposition in dust particles has important impact on biological primary marine productivity in subarctic Pacific.

References

Athanasopoulou, E., Tombrou, M., Pandis, S. N., and Russell, A. G.: The role of sea-salt emissions and heterogeneous chemistry in the air quality of polluted coastal areas, Atmos. Chem. Phys., 8, 5755–5769, doi:10.5194/acp-8-5755-2008, 2008.

Bauer, S. E., Balkanski, Y., Schulz, M., Hauglustaine, D. A., and Dentener, F.: Global modeling of heterogeneous chemistry on mineral aerosol surfaces: Influence on tropospheric ozone chemistry and comparison to observations, J. Geophys. Res-Atmos., 109, D02304, doi:10.1029/2003JD003868, 2004.

Byun, D. W. and Dennis, R.: Design Artifacts in Eulerian Air-Quality Models – Evaluation of the

Effects of Layer Thickness and Vertical Profile Correction on Surface Ozone Concentrations, Atmos. Environ., 29, 105–126, 1995.

Choi, J. C., Lee, M., Chun, Y., Kim, J., and Oh, S.: Chemical composition and source signature of spring aerosol in Seoul, Korea, J. Geophys. Res.-Atmos., 106, 18067–18074, 2001.

Deng, Z., Han, Y., Bai, H., and Zhao, T.: Effect of dust aerosol production in China mainland on marine primary productivity, China Environmental Science, 28, 872–876, 2008 (in Chinese).

Duce, R. A., Unni, C. K., Ray, B. J., Prospero, J. M., and Merrill, J. T.: Long-range atmospheric of soil dust from Asia to the tropical North Pacific: temporal variability., Science, 209, 1522–1524, 1980.

Duckworth, O. W. and Martin, S. T.: Surface complexation and dissolution of hematite by C-1-C-6 dicarboxylic acids at pH=5.0, Geochim. Cosmochim. Ac., 65, 4289–4301, 2001.

Evans, M. J. and Jacob, D. J.: Impact of new laboratory studies of N_2O_5 hydrolysis on global model budgets of tropospheric nitrogen oxides, ozone, and OH, Geophys. Res. Lett., 32, L09813, doi:10.1029/2005GL022469, 2005.

Fan, S. M., Moxim, W. J., and Levy, H.: Aeolian input of bioavailable iron to the ocean, Geophys. Res. Lett., 33, L07602, doi:10.1029/2005GL024852, 2006.

Gratpanche, F. a. J. P. S.: Uptake coefficients of NO_3 radicals, J. Chim. Phys., 96, 213–231, 1996.

Guimbaud, C., Arens, F., Gutzwiller, L., Gggeler, H. W., and Ammann, M.: Uptake of HNO_3 to deliquescent sea-salt particles: a study using the short-lived radioactive isotope tracer 13N, Atmos. Chem. Phys., 2, 249–257, doi:10.5194/acp-2-249-2002, 2002.

He, K. B., Huo, H., and Zhang, Q.: Urban air pollution in China: current status, characteristics, and progress, Annu. Rev. Energy Env., 27, 397–431, 2002.

Imai, K., Nojiri, Y., Tsurushima, N., and Saino, T.: Time series of seasonal variation of primary productivity at station KNOT (44 degrees N, 155 degrees E) in the sub-arctic western North Pacific, Deep-Sea Res. Pt. Ii., 49, 5395–5408, 2002.

Jacob, D. J.: Heterogeneous chemistry and tropospheric ozone, Atmos. Environ., 34, 2131–2159, 2000.

Jordan, C. E., Dibb, J. E., Anderson, B. E., and Fuelberg, H. E.: Uptake of nitrate and sulfate on dust aerosols during TRACE-P, J. Geophys. Res.-Atmos., 108, 8817, doi:10.1029/2002JD003101, 2003.

Kanaya, Y., Pochanart, P., Liu, Y., Li, J., Tanimoto, H., Kato, S., Suthawaree, J., Inomata, S., Taketani, F., Okuzawa, K., Kawamura, K., Akimoto, H., and Wang, Z. F.: Rates and regimes

A model case study of a super-duststorm in March 2010

J. Li et al.

Title Page

Abstract | Introduction

Conclusions | References

Tables | Figures

◄ | ►►

◄ | ►

Back | Close

Full Screen / Esc

Printer-friendly Version

Interactive Discussion

of photochemical ozone production over Central East China in June 2006: a box model analysis using comprehensive measurements of ozone precursors, Atmos. Chem. Phys., 9, 7711–7723, doi:10.5194/acp-9-7711-2009, 2009.

Kim, B. G. and Park, S. U.: Transport and evolution of a winter-time Yellow sand observed in Korea, Atmos. Environ., 35, 3191–3201, 2001.

Kotamarthi, V. R., Gaffney, J. S., Marley, N. A., and Doskey, P. V.: Heterogeneous NO_x chemistry in the polluted PBL, Atmos. Environ., 35, 4489–4498, 2001.

Krueger, B. J., Grassian, V. H., Cowin, J. P., and Laskin, A.: Heterogeneous chemistry of individual mineral dust particles from different dust source regions: the importance of particle mineralogy, Atmos. Environ., 38, 6253–6261, 2004.

Lasserre, F., Cautenet, G., Bouet, C., Dong, X., Kim, Y. J., Sugimoto, N., Matsui, I., and Shimizu, A.: A model tool for assessing real-time mixing of mineral and anthropogenic pollutants in East Asia: a case study of April 2005, Atmos. Chem. Phys., 8, 3603–3622, doi:10.5194/acp-8-3603-2008, 2008.

Li, J., Wang, Z. F., Akimoto, H., Gao, C., Pochanart, P., and Wang, X. Q.: Modeling study of ozone seasonal cycle in lower troposphere over east Asia, J. Geophys. Res-Atmos., 112, D22S25, doi:10.1029/2006JD008209, 2007.

Li, J., Wang, Z., Akimoto, H., Yamaji, K., Takigawa, M., Pochanart, P., Liu, Y., Tanimoto, H., and Kanaya, Y.: Near-ground ozone source attributions and outflow in central eastern China during MTX2006, Atmos. Chem. Phys., 8, 7335–7351, doi:10.5194/acp-8-7335-2008, 2008.

Li, J., Wang, Z., Wang, X., Yamaji, K., Takigawa, M., Kanaya, Y., Pochanart, P., Liu, Y., Irie, H., Hu, B., Tanimoto, H., and Akimoto, H.: Impacts of aerosols on summertime tropospheric photolysis frequencies and photochemistry over Central Eastern China, Atmos. Environ., 45, 1817–1829, 2011a.

Li, J. W., Han, Z. W., and Zhang, R. J.: Model study of atmospheric particulates during dust storm period in March 2010 over East Asia, Atmos. Environ., 45, 3954–3964, doi:10.1016/j.atmosenv.2011.04.068, 2011b.

Luo, C., Mahowald, N. M., Meskhidze, N., Chen, Y., Siefert, R. L., Baker, A. R., and Johansen, A. M.: Estimation of iron solubility from observations and a global aerosol model, J. Geophys. Res-Atmos., 110, D23307, doi:10.1029/2005JD006059, 2005.

Malm, W. C., Day, D. E., and Kreidenweis, S. M.: Light scattering characteristics of aerosols as a function of relative humidity: Part I – A comparison of measured scattering and aerosol concentrations using the theoretical models, J. Air Waste Manage, 50, 686–700, 2000.

A model case study of a super-duststorm in March 2010

J. Li et al.

Martin, J. H. and Fitzwater, S. E.: Iron deficiency limits phytoplankton growth in the North-east Pacific subarctic, Nature, 331, 341–343, 1988.

Martin, R. V., Jacob, D. J., Yantosca, R. M., Chin, M., and Ginoux, P.: Global and regional decreases in tropospheric oxidants from photochemical effects of aerosols, J. Geophys. Res.-Atmos., 108, 4097, doi:10.1029/2002JD002622, 2003.

Meskhidze, N., Chameides, W. L., Nenes, A., and Chen, G.: Iron mobilization in mineral dust: Can anthropogenic SO2 emissions affect ocean productivity?, Geophys. Res. Lett., 30, 2085, doi:10.1029/2003GL018035, 2003.

Nenes, A., Pandis, S. N., and Pilinis, C.: ISORROPIA: A new thermodynamic equilibrium model for multiphase multicomponent inorganic aerosols, Aquat. Geochem., 4, 123–152, 1998.

Ohara, T., Akimoto, H., Kurokawa, J., Horii, N., Yamaji, K., Yan, X., and Hayasaka, T.: An Asian emission inventory of anthropogenic emission sources for the period 1980–2020, Atmos. Chem. Phys., 7, 4419–4444, doi:10.5194/acp-7-4419-2007, 2007.

Phadnis, M. J. and Carmichael, G. R.: Numerical investigation of the influence of mineral dust on the tropospheric chemistry of East Asia, J. Atmos. Chem., 36, 285–323, 2000.

Pradhan, M., Kyriakou, G., Archibald, A. T., Papageorgiou, A. C., Kalberer, M., and Lambert, R. M.: Heterogeneous uptake of gaseous hydrogen peroxide by Gobi and Saharan dust aerosols: a potential missing sink for H_2O_2 in the troposphere, Atmos. Chem. Phys., 10, 7127–7136, doi:10.5194/acp-10-7127-2010, 2010.

Song, C. H. and Carmichael, G. R.: A three-dimensional modeling investigation of the evolution processes of dust and sea-salt particles in east Asia, J. Geophys. Res.-Atmos., 106, 18131–18154, 2001.

Sugimoto, N., Matsui, I., Shimizu, A., Uno, I., Asai, K., Endoh, T., and Nakajima, T.: Observation of dust and anthropogenic aerosol plumes in the Northwest Pacific with a two-wavelength polarization lidar on board the research vessel Mirai, Geophys. Res. Lett., 29, 1901, doi:10.1029/2002GL015112, 2002.

Sun, Y. L., Zhuang, G. S., Wang, Y., Zhao, X. J., Li, J., Wang, Z. F., and An, Z. S.: Chemical composition of dust storms in Beijing and implications for the mixing of mineral aerosol with pollution aerosol on the pathway, J. Geophys. Res.-Atmos., 110, D24209, doi:10.1029/2005JD006054, 2005.

Sunda, W. G. and Huntsman, S. A.: Interrelated influence of iron, light and cell size on marine phytoplankton growth, Nature, 390, 389–392, 1997.

Tang, Y. H., Carmichael, G. R., Kurata, G., Uno, I., Weber, R. J., Song, C. H., Guttikunda, S. K.,

Title Page

Abstract | Introduction

Conclusions | References

Tables | Figures

◄◄ | ►►

◄ | ►

Back | Close

Full Screen / Esc

Printer-friendly Version

Interactive Discussion

Woo, J. H., Streets, D. G., Wei, C., Clarke, A. D., Huebert, B., and Anderson, T. L.: Impacts of dust on regional tropospheric chemistry during the ACE-Asia experiment: A model study with observations, J. Geophys. Res.-Atmos., 109, D19S21, doi:10.1029/2003JD003806, 2004.

Tie, X. X., Madronich, S., Walters, S., Edwards, D. P., Ginoux, P., Mahowald, N., Zhang, R. Y., Lou, C., and Brasseur, G.: Assessment of the global impact of aerosols on tropospheric oxidants, J. Geophys. Res-Atmos., 110, D03204, doi:10.1029/2004JD005359, 2005.

Uno, I., Wang, Z., Chiba, M., Chun, Y. S., Gong, S. L., Hara, Y., Jung, E., Lee, S. S., Liu, M., Mikami, M., Music, S., Nickovic, S., Satake, S., Shao, Y., Song, Z., Sugimoto, N., Tanaka, T., and Westphal, D. L.: Dust model intercomparison (DMIP) study over Asia: Overview, J. Geophys. Res-Atmos., 111, D12213, doi:10.1029/2005JD006575, 2006.

Vlasenko, A., Sjogren, S., Weingartner, E., Stemmler, K., Gäggeler, H. W., and Ammann, M.: Effect of humidity on nitric acid uptake to mineral dust aerosol particles, Atmos. Chem. Phys., 6, 2147–2160, doi:10.5194/acp-6-2147-2006, 2006.

Walcek, C. J. and Aleksic, N. M.: A simple but accurate mass conservative, peak-preserving, mixing ratio bounded advection algorithm with Fortran code, Atmos. Environ., 32, 3863–3880, 1998.

Wang, Q. Z., Zhuang, G. S., Li, J. A., Huang, K., Zhang, R., Jiang, Y. L., Lin, Y. F., and Fu, J. S.: Mixing of dust with pollution on the transport path of Asian dust – Revealed from the aerosol over Yulin, the north edge of Loess Plateau, Sci. Total. Environ., 409, 573–581, 2011a.

Wang, S. H., Tsay, S. C., Lin, N. H., Hsu, N. C., Bell, S. W., Li, C., Ji, Q., Jeong, M. J., Hansell, R. A., Welton, E. J., Holben, B. N., Sheu, G. R., Chu, Y. C., Chang, S. C., Liu, J. J., and Chiang, W. L.: First detailed observations of long-range transported dust over the northern South China Sea, Atmos. Environ., 45, 4804–4808, 2011b.

Wang, Z. F., Ueda, H., and Huang, M. Y.: A deflation module for use in modeling long-range transport of yellow sand over East Asia, J. Geophys. Res.-Atmos., 105, 26947–26959, 2000.

Wang, Z. F., Akimoto, H., and Uno, I.: Neutralization of soil aerosol and its impact on the distribution of acid rain over east Asia: Observations and model results, J. Geophys. Res-Atmos., 107, 4389, doi:10.1029/2001JD001040, 2002.

Wang, Z. F., Li, J., Wang, X. Q., Pochanart, P., and Akimoto, H.: Modeling of regional high ozone episode observed at two mountain sites (Mt. Tai and Huang) in East China, J. Atmos. Chem., 55, 253–272, 2006.

Wei, C.: Modeling the effects of heterogeneous reactions on atmospheric chemistry and aerosol properties, PhD, Chemical and Biochemical Engineering in the Graduate College

A model case study of a super-duststorm in March 2010

J. Li et al.

Title Page

Abstract	Introduction
Conclusions	References
Tables	Figures

◀◀ ▶▶

◀ ▶

Back Close

Full Screen / Esc

Printer-friendly Version

Interactive Discussion

University of Iowa, Iowa City, Iowa, 2010.

Wesely, M. L.: Parameterization of Surface Resistances to Gaseous Dry Deposition in Regional-Scale Numerical-Models, Atmos. Environ., 23, 1293–1304, 1989.

Wilkening, K. E., Barrie, L. A., and Engle, M.: Atmospheric science – Trans-Pacific air pollution, Science, 290, 65–67, 2000.

Yuan, H., Zhuang, G. S., Li, J., Wang, Z. F., and Li, J.: Mixing of mineral with pollution aerosols in dust season in Beijing: Revealed by source apportionment study, Atmos. Environ., 42, 2141–2157, 2008.

Yue, X., Wang, H. J., Liao, H., and Fan, K.: Simulation of dust aerosol radiative feedback using the GMOD: 2. Dust-climate interactions, J. Geophys. Res.-Atmos., 115, D10202, doi:10.1029/2008JD010995, 2010.

Zaveri, R. A. and Peters, L. K.: A new lumped structure photochemical mechanism for large-scale applications, J. Geophys. Res.-Atmos., 104, 30387–30415, 1999.

Zhang, D., Zang, J., Shi, G., Iwasaka, Y., Matsuki, A., and Trochkine, D.: Mixture state of individual Asian dust particles at a coastal site of Qingdao, China, Atmos. Environ., 37, 3895–3901, doi:10.1016/s1352-2310(03)00506-5, 2003.

Zhang, X. Y., Zhuang, G. S., Chen, J. M., and Xue, H. X.: Speciation of the elements and compositions on the surfaces of dust storm particles: The evidence for the coupling of iron with sulfur in aerosol during the long-range transport, Chinese Sci. Bull., 50, 738–744, 2005.

Zhao, J. P., Zhang, F. W., Xu, Y., Chen, J. S., Yin, L. Q., Shang, X. S., and Xu, L. L.: Chemical Characteristics of Particulate Matter during a Heavy Dust Episode in a Coastal City, Xiamen, 2010, Aerosol Air Qual. Res., 11, 300–309, 2011.

Zheng, C. (Ed.): Atlas of Soil Environmental Background Value in the People's Republic of China, China Environmental Science Press, Beijing, China, 1994.

Zhu, H. and Zhang, H. S.: An estimation of the threshold friction velocities over the three different dust storm source areas in northwest China, Acta. Meteorol. Sin., 68, 977–984, 2010 (in Chinese).

Zhu, S., Butler, T., Sander, R., Ma, J., and Lawrence, M. G.: Impact of dust on tropospheric chemistry over polluted regions: a case study of the Beijing megacity, Atmos. Chem. Phys., 10, 3855–3873, doi:10.5194/acp-10-3855-2010, 2010.

Zhuang, G. S., Yi, Z., and Duce, R.: Link between iron and sulfur cycles suggested by detection of iron(II) in remote marine aerosols, Nature, 355, 537–539, 1992.

Zhuang, G. S., Guo, J. H., Yuan, H., and Zhang, X. Y.: Coupling and feedback between iron

Title Page

Abstract | Introduction

Conclusions | References

Tables | Figures

◄ | ►

◄ | ►

Back | Close

Full Screen / Esc

Printer-friendly Version

Interactive Discussion

and sulphur in air-sea exchange, Chinese Sci. Bull., 48, 1080–1086, 2003.

Zhuang, G. S., Zhang, W. J., Huang, K., Li, J. A., Zhang, R., Wang, Q. Z., Sun, Y. L., Fu, J. S., Chen, Y., Xu, D. Q., and Wang, W.: Mixing and transformation of Asian dust with pollution in the two dust storms over the northern China in 2006, Atmos. Environ., 44, 3394–3403, 2010.

A model case study of a super-duststorm in March 2010

J. Li et al.

◄◄ | ►►

◄ | ►

Back | Close

Full Screen / Esc

Table 1. Heterogeneous reactions and reactive uptake coefficients.

No.	Heterogeneous reactions	γ^a	Ref[b]
HR1	$N_2O_5+\text{sulfate}\rightarrow 2HNO_3$	$\gamma = \alpha \times 10^{\beta}$ $\alpha = 2.79 \times 10^{-4} + 1.3$ $\times 10^{-4} \times RH - 3.43 \times 10^{-6}$ $\times RH^2 + 7.52 \times 10^{-9} \times RH^3$ $\beta = 4 \times 10^{-2} \times (T-294)(T \geq 282\,\text{K})$ $\beta = -0.48(T < 282\,\text{K})$	1
HR2	$NO_3+\text{sulfate}\rightarrow HNO_3$	3×10^{-2}	2
HR3	$HO_2+\text{sulfate}\rightarrow 0.5H_2O_2$	2.5×10^{-1}	3
HR4	$OH+\text{sulfate}\rightarrow \text{products}$	2×10^{-1}	4
HR5	$HCHO+\text{sulfate}\rightarrow \text{products}$	2.2×10^{-2}	5
HR6	$O_3+\text{soot}\rightarrow \text{products}$	$1.8 \times 10^{-4} \times e^{-\frac{1000}{T}}$	5
HR7	$NO_2+\text{soot}\rightarrow HONO$	3.3×10^{-4}	6
HR8	$HNO_3+\text{soot}\rightarrow NO_2$	2.1×10^{-2}	6
HR9	$NO_2+\text{soot}\rightarrow 0.5HONO+0.5HNO_3$	3×10^{-3}	7
HR10	$N_2O_5+\text{soot}\rightarrow 2HNO_3$	5×10^{-3}	1
HR11	$O_3+\text{dust}\rightarrow \text{products}$	2.7×10^{-5}	8
HR12	$HNO_3+\text{dust}\rightarrow NO_3^-$	$\gamma = \frac{c \times RH}{(1-RH) \times (1-(1-c) \times RH)} \times 0.018(c=8)$	9,10[c]
HR13	$NO_2+\text{dust}\rightarrow 0.5HONO+0.5HNO_3$	2.1×10^{-6}	8
HR14	$NO_3+\text{dust}\rightarrow HNO_3$	1×10^{-3}	11
HR15	$N_2O_5+\text{dust}\rightarrow 2HNO_3$	3×10^{-2}	8
HR16	$OH+\text{dust}\rightarrow \text{products}$	1×10^{-1}	8
HR17	$HO_2+\text{dust}\rightarrow 0.5H_2O_2$	2×10^{-1}	8
HR18	$H_2O_2+\text{dust}\rightarrow \text{products}$	$\gamma = 12 \times RH^2 - 5.95 \times RH + 4.08$	12
HR19	$SO_2+\text{dust}\rightarrow SO_4^{2-}$	1×10^{-4}	13
HR20	$CH_3COOH+\text{dust}\rightarrow \text{products}$	1×10^{-3}	8
HR21	$CH_3OH+\text{dust}\rightarrow \text{products}$	1×10^{-5}	8

Table 1. Continued.

No.	Heterogeneous reactions	γ[a]	Ref[b]
HR22	HCHO+dust→products	1×10^{-5}	8
HR23	N_2O_5+SSA→2HNO$_3$	5×10^{-3}(RH < 62 %) 3×10^{-2}(RH ≥ 62 %)	1
HR24	NO_3+SSA→HNO$_3$	1×10^{-3}	7
HR25	HO_2+SSA→0.5H$_2$O$_2$	2×10^{-1}	7
HR26	SO_2+SSA→SO$_4^{2-}$	5×10^{-3}(RH < 50 %) 5×10^{-2}(RH ≥ 50 %)	14
HR27	NO_3+SSA→NO$_3^-$	1.7×10^{-2}	15
HR28	HNO_3+SSA→NO$_3^-$	5×10^{-1}	16

[a] γ is the reaction probability; T is temperature(K), RH is relative humidity (%)

[b] References:
1: Evans and Jacob (2005); 2: Bauer et al. (2004); 3: Kanaya et al. (2009); 4:Tie and Brasseur (1999); 5: Tie et al. (2005); 6: Kotamarthi et al. (2001); 7: Jacob (2000); 8: Zhu et al. (2010); 9: Vlasenko et al. (2006); 10: Wei (2010); 11: Martin et al. (2003); 12: Pradhan et al. (2010); 13: Phadnis and Carmichael (2000); 14: Song and Carmichael (2001); 15: Gratpanche (1996); 16: Guimbaud et al. (2002).

[c] Vlasenko et al. in refrence 9# suggested the BET isotherm has a similar shape with the experimental γ as a function of RH. Wei et al. in refrence 10# reported γ on China Losses at 0 %, 40 % and 80 % RH. So γ in this study is calculated by the BET isotherm forced by γ values reported by Wei (2010).

Table 2. Observed and simulated mass fractions (%) of fine and coarse particles at Shanghai and Xiamen during the dust episode.

		Obs	Mod
Shanghai			
	Fine($<2.5\,\mu$m)	18.9	33.2
	Coarse($>2.5\,\mu$m)	81.1	66.8
Xiamen			
	Fine($<2.5\,\mu$m)	43.0	47.9
	Coarse($>2.5\,\mu$m)	57.0	52.1

Full Screen / Esc

Printer-friendly Version

Interactive Discussion

Table 3. Atmospheric deposition Fluxes of Fe(II) to the ocean in the model domain during 19–22 March 2010 in the base (mixing processes) and sensitivity (no mixing processes) simulations.

	Dry deposition	Wet deposition	Total deposition
Base(ton)	128	199	327
Sensitivity(ton)	51	20	71
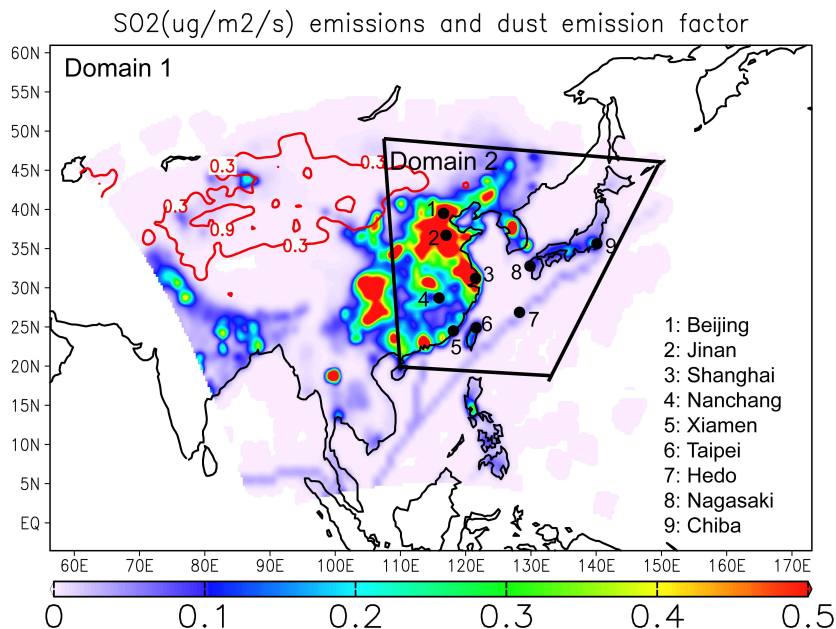
Fig. 1. Distribution of SO$_2$ emission rate ($\mu g\,m^{-2}\,s^{-1}$) in this study and modeling domain of NAQPMS. Also shown are the weighting factor of dust emissions (E in Eq. (1), red contours) and observed stations (solid cycles). The numerical characters mean the locations and name in the study.
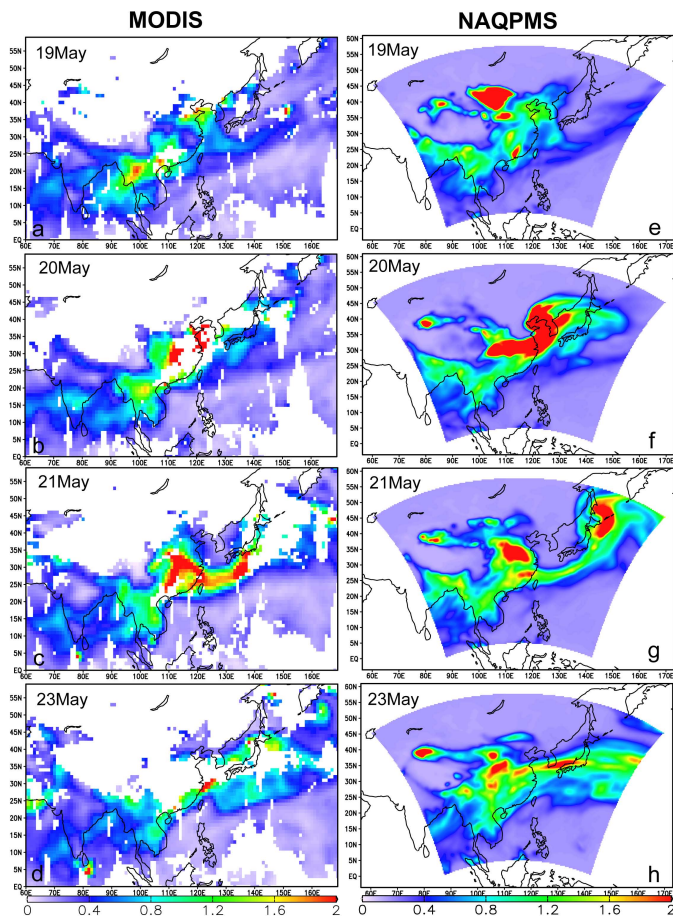
Fig. 2. MODIS-derived (left panel) and simulated AOD550 (right panel) during 19–23 March 2010. The white color in left panel indicates cloud contaminations.
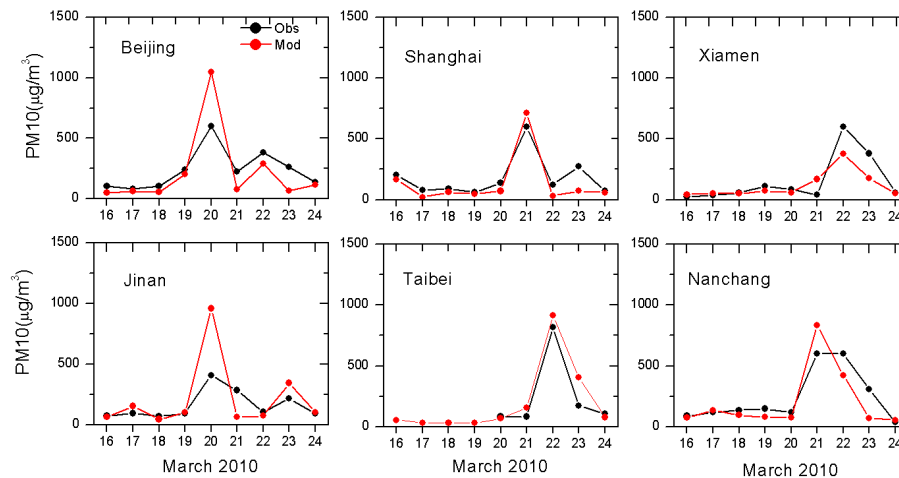
Fig. 3. Observed (black) and simulated (red) daily mean PM$_{10}$ concentrations at six stations in China during 15–24 March 2010.
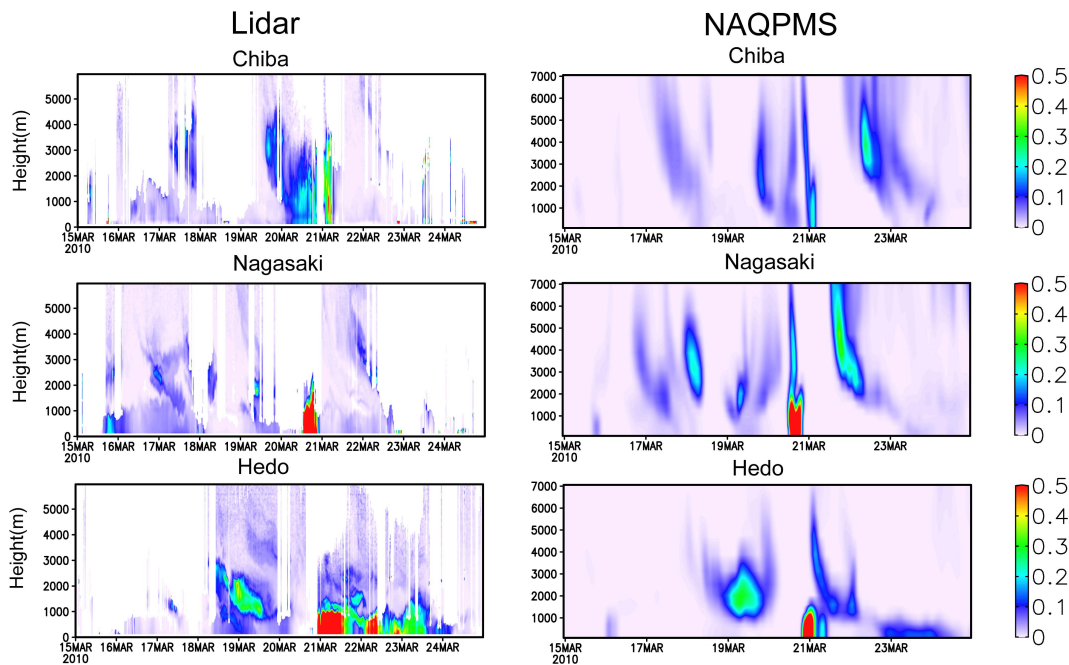
Fig. 4. Lidar measurements (532 nm) (left panel) and simulations (550 nm) (right panel) of extinction coefficients during 15–24 March 2010 at Chiba, Nagasaki and Hedo.
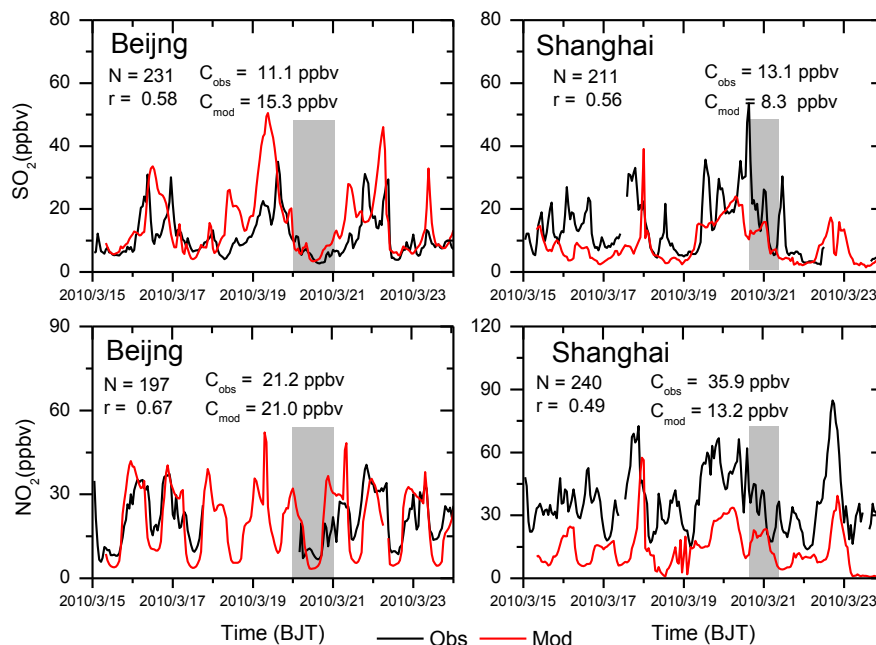
Fig. 5. Observed (black) and simulated (red) concentrations (ppbv) of SO_2 (upper panel) and NO_2 (lower panel) at Beijing (left panel) and Shanghai (right panel) during 15–24 March 2010. N and r represent numbers of paired samples and correlation coefficients, respectively. C_{obs} and C_{mod} are average concentrations of observed and modeled species. The gray shades are the periods in the duststorm episode at two cities.
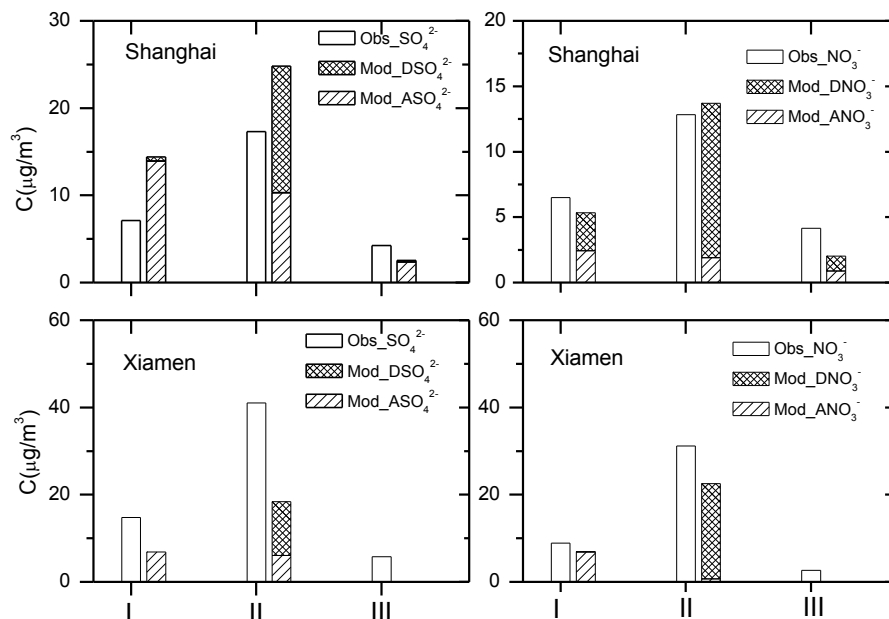
Fig. 6. Observed and simulated sulfate (left panel) and nitrate (right panel) at Shanghai (upper) and Xiamen (lower) during pre-dust (I), dust (II) and after-dust (III) period. DSO_4^{2-} and DNO_3^- (same as below) are sulfate and nitrate captured by dust particles by heterogeneous chemistry, respectively. ASO_4^{2-} a nd ANO_3^- represent the sulfate and nitrate particles by anthropogenic emissions. Observations at Xiamen are from Zhao et al. (2011).
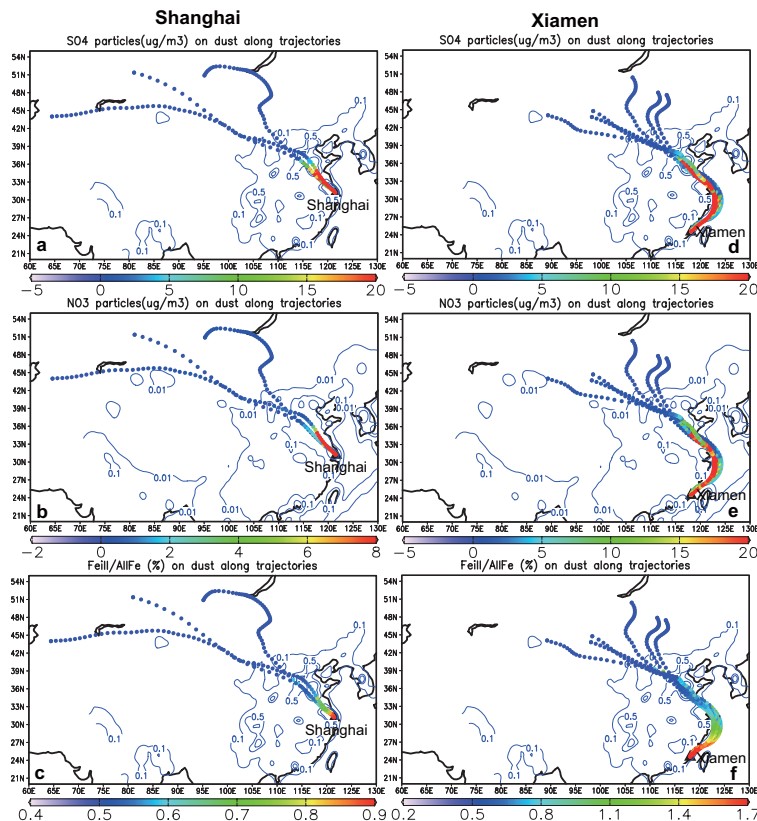
Fig. 7. Simulated sulfate (**a** and **d**) and nitrate (**c** and **e**) ($\mu g\,m^{-3}$) captured by dust particles by heterogeneous chemistry along the 3-day back-trajectories at Shanghai and Xiamen during the dusty periods. Also shown is the mass fraction of dissolved Fe (Fe(II)) in total Fe (e and f). The contours represent the SO_2 (**a**, **c**, **d** and **f**) and NO_x (**b** and **e**) emission rate ($\mu g\,m^{-2}\,s^{-1}$).
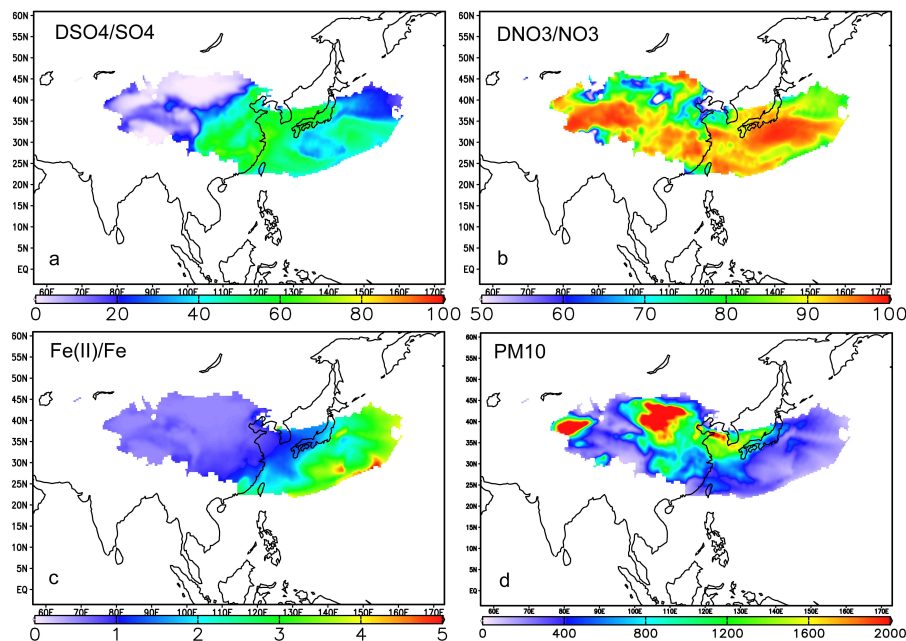
Fig. 8. Percentages of surface DSO_4^{2-} **(a)** and DNO_3^- **(b)** in total sulfate and nitrate during dusty periods over East Asia. Also shown are the fraction (%) of Fe(II) in total Fe **(c)** and surface PM_{10} concentration ($\mu g\,m^{-3}$) **(d)**.
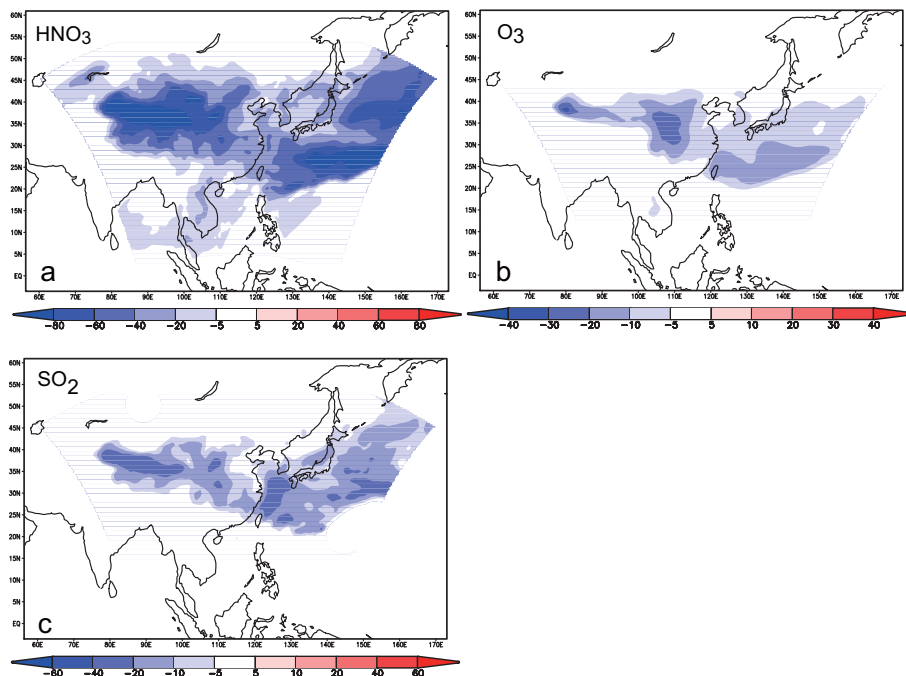
Fig. 9. Averaged dust influences (%) on surface HNO_3 **(a)**, O_3 **(b)** and SO_2 **(c)** concentrations over East Asia during 19–22 March 2010.
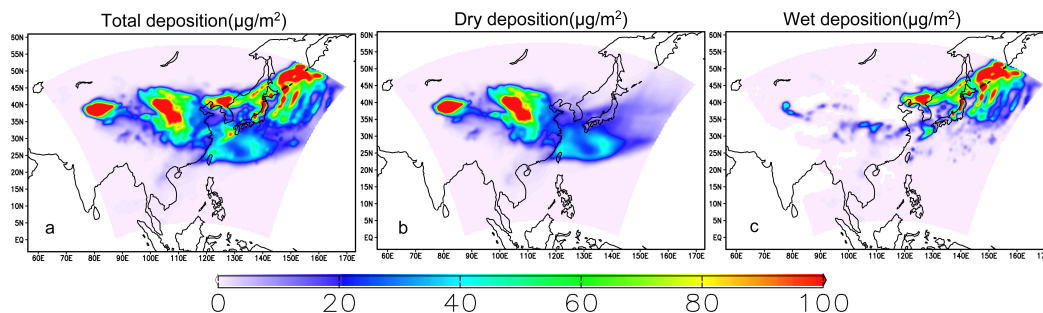
Fig. 10. Simulated **(c)** total deposition ($\mu g\,m^{-2}$), **(b)** dry deposition ($\mu g\,m^{-2}$), **(c)** wet deposition ($\mu g\,m^{-2}$) of Fe(II) over East Asia during 19–22 March 2010.